Awakening Collective Wisdom: Elevating Super-Resolution Network Generalization through Cooperative Game Theory

Anonymous authors
Paper under double-blind review

Abstract

Improving the generalization capability of image super-resolution algorithms is a fundamental challenge when deploying them in real-world scenarios. Prior methods often relied on the assumption that training on diverse data can improve generalization capabilities, leading to the development of complex degradation models that simulate real-world degradation. Unlike previous works, we present a novel training strategy grounded in cooperative game theory to improve the generalization capacity of existing image super-resolution algorithms. Within this framework, we conceptualize all neurons in the network as participants engaged in a cooperative relationship, where their collective responses determine the final prediction. As a solution, we propose to awaken suppressed neurons that hinder the generalization capability through our **E**rase-and-**A**waken **T**raining **S**trategy (**EATS**), thus fostering equitable contributions among all neurons and effectively improving generalization performance. EATS offers several compelling benefits. *1) Seamless integration with existing architectures*: It integrates with existing networks to enhance their generalization capability for unseen scenarios. *2) Theoretically feasible strategy*: We theoretically prove the effectiveness of our strategy in enhancing the Shapley value (reflecting each participant's contributions to prediction). *3) Consistent performance improvements*: Comprehensive experiments on various challenging datasets consistently demonstrate performance improvements when employing our strategy. The code will be publicly available.

1 Introduction

Single image super-resolution (SR) is a classical low-level vision task that focuses on restoring a high-resolution (HR) image from a low-resolution (LR) version. Recently, deep learning-based SR (Dong et al., 2015; Zhang et al., 2018b; 2019; 2018a; Chen et al., 2022; Zhang et al., 2022; Wang et al., 2023; Zhang et al., 2022) algorithms have made significant efforts in synthetic environments. However, overfitting to specific degradations in synthetic scenarios leads to poor generalization performance when deploying these algorithms in real-world scenarios due to domain gaps.

In response to the mentioned challenge, some efforts have been devoted to diversify the synthetic training data to encompass the broader space of real-world degradation, thereby enhancing the generalization capabilities of SR models. For example, BSRGAN (Zhang et al., 2021) introduced a complex degradation model involving a random shuffle of degradation orders, while Real-ESRGAN (Wang et al., 2021) introduced second-order degradation techniques. However, these efforts operate under the assumption that diversifying the training data can indeed improve generalization capabilities. In contrast to previous works, we contemplate a shift in focus from data to optimization, aiming to present a flexible training paradigm that fosters the generalization capability of algorithms.

Observation. To achieve this goal, we conduct an initial exploration into the properties of algorithms when applied to in-the-wild scenes. The co-adaption phenomenon, discussed in this work, Hinton et al. (2012), provides fundamental insights for our investigation. It suggests that training over-parameterized networks often leads to the over-activation of specific neuronal connections while inhibiting others. However, when exposed to unseen real-world scenarios, these established

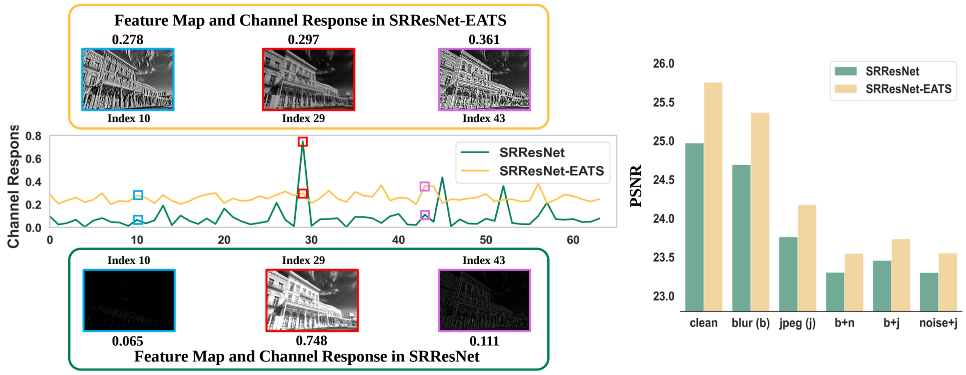

(a) Channel Response

(b) Generalization

Figure 1: The Erase-and-Awaken Training Strategy (EATS) mitigates the co-adaption problem by promoting equitable contributions among all filters, thereby improving generalization performance. (a) Co-adaption in SR: We analyze channel responses in unseen scenarios, averaging channel responses from the 2^{nd} block in SRResNet (Ledig et al., 2017) (trained on Five5K (Bychkovsky et al., 2011)) across 100 randomly sampled unseen images. We visualize the feature maps and responses of channel index 10, 29, and 43. It reveals the co-adaption phenomenon (Hinton et al., 2012), where a few channels are highly activated while others are inhibited, resulting in poor generalization. In contrast, integrating EATS with SRResNet achieves equitable and activated channel responses. (b) Generalization performance: Results on Set5 with ×4 scaling under different degradation settings, showcasing the effectiveness of EATS in improving the network's generalization capacity.

connections perform inadequately than on the training data, thus limiting the network's generalization capacity. To verify this phenomenon within the SR task, we investigate the average response of each channel within the same layer on unseen data scenarios. As depicted in Fig. 1(a), we observe that only a few channel responses are highly activated while the majority remain inhibited. These dormant channels represent a critical factor hindering algorithms' generalization performance. This finding leads to a pivotal question: "How can we 'awaken' these dormant channels and encourage equitable contributions among all filters to prediction for improving the generalization capacity?"

Solution. In this paper, we introduce cooperative game theory to tackle the generalization challenges in SR algorithms. We present a novel training strategy, denoted as Erase-and-Awaken Training Strategy (EATS), which offers a distinctive perspective by viewing all neurons within the network as active participants engaged in a collaborative relationship. Within these networks, intertwined with complex neuronal connections, their combined responses harmoniously converge to ascertain the ultimate prediction. To awaken the inhibited participants that hinder generalization performance, we propose to randomly perturb the responses of the neurons and maximize their contributions to the prediction. As presented in Fig. 1(a), averaged responses of the initially inhibited channel (index 10 and 43) have been awakened while an abnormally highly activated channel (index 29) was suppressed. It demonstrates the ability of EATS to promote equitable contributions from all channels to the network's prediction but also attain consistent channel response distribution on unseen images. Furthermore, in Fig. 1(b), we provide quantitative evidence to show the effectiveness of our EATS strategy in boosting algorithm's generalization performance on unseen multi-degraded scenarios.

The main contributions of this work are summarized as follows: (1) We propose a novel training strategy grounded in cooperative game theory, fostering equitable contributions among all neurons to enhance the generalization capacity of SR algorithms. (2) Our EATS can seamlessly integrate into existing super-resolution networks, providing a flexible and effective training paradigm. Theoretical proof substantiates the effectiveness of our strategy in improving the Shapley value (measuring each participant's contribution to predictions). (3) Extensive experiments conducted on various challenging datasets consistently demonstrate performance improvements via employing our strategy.

2 Related work

Super-Resolution. Image super-resolution task focuses on restoring a high-resolution image from its corrupted low-resolution counterpart. Conventional SR networks (Dong et al., 2014; Dai et al., 2019a; Kim et al., 2016; Lim et al., 2017; Wang et al., 2018a; Yuan et al., 2018; Dai et al., 2019b; Xia et al., 2022; Lai et al., 2017; Sajjadi et al., 2017; Johnson et al., 2016; Ma et al., 2020; Liu et al., 2020; Zhou et al., 2020; Magid et al., 2021) are typically trained on image pairs generated via bicubic interpolation. However, it may induce overfitting towards the specific degradation, resulting in limited generalization in real-world degradations. As a solution, a blind SR paradigm involving degradation prediction and super-resolution is introduced to tackle complex real-world scenarios. IKC Gu et al. (2019) introduces a predict-and-correct principle, *i.e.*, iteratively correcting the estimated kernel based on the previous SR results. DAN (Huang et al., 2020) proposes an alternating optimization algorithm for estimating blur kernel and restoring super-resolved image iteratively. Nevertheless, these techniques are confined to addressing conditions outlined within the predefined degradation model and often exhibit sub-optimal generalization when encountering images that deviate from the degradation model. Therefore, the alternative approach involves enriching the training set with random combinations of diverse degradations, such as the high-order degradation process in Real-ESRGAN (Wang et al., 2021) and the degradation shuffle strategy in BSRGAN (Zhang et al., 2021). However, the aforementioned methods exclusively simulate real-world scenarios by predicting degradations within the predefined model and augmenting the diversity of training data while neglecting the exploration of more streamlined training strategies.

Generalization in low-level vision. Since the degradations encountered during the training phase cannot faithfully simulate the complicated degradations inherent in real-world scenarios, the challenge of generalization in low-level tasks has garnered significant attention. In terms of the generalization assessment, Liu et al. (2021) introduces a deep degradation representation as an approximate evaluation metric for measuring generalization ability, where the worse the degradation clustering effect means the better generalizability. SRGA Liu et al. (2022) delves into the statistical attributes of internal features within deep networks to measure their generalization capability. Moreover, many researchers are dedicated to improving the generalizability of networks. Kong et al. (2022) broke the common sense that dropout cannot be effectively applied to low-level vision and explored its working mechanism in SR. Li et al. (2023) introduced a causality training strategy that focuses on learning the distortion-invariant representations, thereby enhancing the generalization capacity.

3 Method

3.1 Preliminary

Shapley value serves as a fundamental tool within cooperative game theory for credit allocation. In cooperative game theory, a game is defined by a set function where each subset's value represents the profit when the associated players participate. Given a cooperative game model, the game consists of a set $\mathcal{N}$ with $|\mathcal{N}|$ individual players, denoted as $\mathcal{N} = \{n_i\}_{i=1}^{i=|\mathcal{N}|}$. The game's profit is assessed using a specific metric denoted as v, which takes subsets $\mathcal{M} \subseteq \mathcal{N}$ as input and generates a profit score. Formally, Shapley values for the i^{th} player are calculated as

$$\phi_{n_i}(\mathcal{M}, v) = \sum_{\mathcal{M} \subseteq \mathcal{N} \setminus \{n_i\}} \frac{|\mathcal{M}|!(|\mathcal{N}| - |\mathcal{M}| - 1)!}{\mathcal{N}!} [v(\mathcal{M} \cup \{n_i\}) - v(\mathcal{M})]. \tag{1}$$

Intuitively, Eq. 1 quantifies the contribution of a specific player n_i, to the overall profits when introducing this player. This quantification averages across all conceivable subsets where n_i can be included. The Shapley value adheres to several rational properties: (1) Additivity: The Shapley value of each player sum to the profits when all players participate. (2) Symmetry: Players with equivalent contributions receive equal Shapley value. (3) Dummy players: Players who make no contribution receive a Shapley value of zero. These properties ensure that Shapley values offer a fair and justifiable method for evaluating contributions in cooperative game theory.

3.2 Proposed Erase-and-Awaken Training Strategy

Our objective is to design a training strategy to alleviate the co-adaption problem in SR algorithms, which impedes the generalization capacity, and promote equitable contributions of each channel to predictions. Considering that the prediction in networks relies on the intricate connections among all filters, we introduce the cooperative game theory to formulate this process. For a fully convolutional neural network, denoted as f_θ, it is composed of L layers, each equipped with $n_{l\in\{1,\ldots,L\}}$ filters, and

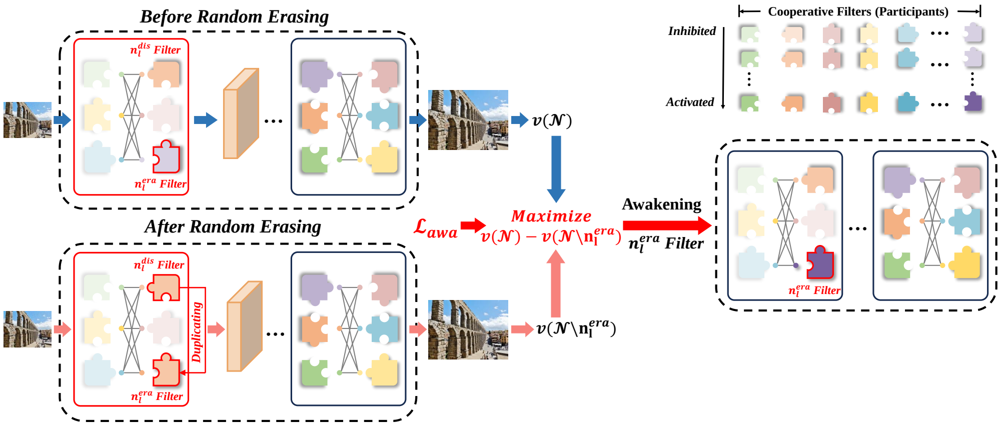

Figure 2: The paradigm of the Erase-and-Awaken Training Strategy (EATS) consists of erasing and awakening steps. **Erasing:** In this step, EATS randomly samples an erased filter and a disruptor filter in a random layer, n_l^{ear} and n_l^{dis} in the l^{th} layer. To assess the contribution of the erased filter, EATS erases n_l^{era} with a duplication of n_l^{dis} and evaluates the performance of networks before and after erasure. **Awakening:** An awakening regularization term, $\mathcal{L}_{awa}$, widens the performance gap before and after erasure, effectively awakening the contribution of the erased filter. Therefore, EATS promotes equitable contributions among filters to predicted high-resolution results and alleviates co-adaption, thereby improving the network's generalization capability.

n_l^i denotes the i^{th} filter in the l^{th} layer. Each filter within the network corresponds to an individual player in the cooperative game model.

Erasing. To assess the contribution of each filter, we first randomly erase a filter and then evaluate the performance gap before and after erasure. Instead of directly dropping the filter to be measured, we opt to randomly sample a disruptor filter within the same layer, and employ the sampled filter to erase it. This approach reduces the correlations among channels and promotes feature diversity, as demonstrated in Section 4.3.1. Formally, we define the erased filter as n_l^{era} and the randomly sampled disruptor as n_l^{dis}. The process of selecting filter nodes n_l^{era} and n_l^{dis} is:

$$\begin{gathered} l = \mathtt{max}\{P(i) \in N[0,1]\}, \quad i \in \{1, ..., L\}, \\ P(n_l^j = n_l^{era}) = \frac{1}{|n_l|}, \quad P(n_l^k = n_l^{dis}) = \frac{1}{|n_l|}, \quad j,k \in \{1,...,|n_l|\}, \quad j \neq k \end{gathered} \tag{2}$$

The networks before and after erasure can be expressed as follows:

$$\begin{gathered} \{n_1^1, ...\}, \{n_l^1, ...n_l^{era}, ..., n_l^{dis}, ...\}, \{n_L^1, ...\} \rightarrow f_\theta, \\ \{n_1^1, ...\}, \{n_1^1, ..., n_l^{dis}, ..., n_l^{dis}, ...\}, \{n_L^1, ...\} \rightarrow f_{\theta'}, \end{gathered} \tag{3}$$

where f_θ denotes the original network and $f_{\theta'}$ represents the network after erasure, $P(\cdot)$ indicates the probability function and $|n_l|$ represents the number of filters in the l^{th} layer.

Awakening. To promote the contribution of the erased filter on the prediction, we introduce an awakening regularization term, $\mathcal{L}_{awa}$, aimed at constraining that the predicted high-resolution image of the disrupted network closely approximates a baseline image. In this paper, the baseline is defined as the upsampled image using bicubic interpolation. Given a low-resolution image, I_{LR}, an upsampled image via bicubic interpolation, I_{Bic}, and the corresponding high-resolution image, I_{HR}, the awakening regularization term is defined as:

$$\mathcal{L}_{awa} = ||f_{\theta'}(I_{LR}) - I_{Bic})||_1, \tag{4}$$

where $||\cdot||_1$ represents ℓ_1 norm. The total loss function of the SR network is formulated as: $\mathcal{L} = \mathcal{L}_{ori} + \mathcal{L}_{awa}$, and $\mathcal{L}_{ori} = ||f_\theta(I_{LR}) - I_{HR})||_1$. The awakening regularization term amplifies the performance gap between the original network and the disrupted network, thus enhancing the contribution of the erased filter, n_l^{era}, on the prediction.

Since all filters among all layers should be active participants in the cooperative game model and contribute equitably to the prediction, we extend the erase-and-awaken training strategy across all

Algorithm 1: Erase-and-Awaken Training Strategy

```
Input: Paired data with $\{I_{LR}, I_{Bic}, I_{HR}\}$, learning rate $\eta$, updated network $f_\theta$ with $L$ layers.
Output: Trained network $f_{\theta^*}$.
while not converge do
    Randomly sample a layer, $l$ from $\{1, \ldots, L\}$ ;
    Randomly sample an erased filter, $n_l^{era}$, and a disruptor filter, $n_l^{dis}$, from $l^{th}$ layer by Eq. 2 ;
    $f_{\theta'} \leftarrow$ Obtained by Eq. 3 ;
    $\mathcal{L}_{awa} \leftarrow ||f_{\theta'}(I_{LR}) - I_{Bic})||_1$ ;
    $\mathcal{L}_{ori} \leftarrow ||f_\theta(I_{LR}) - I_{HR})||_1$ ;
    Update $\theta \leftarrow \theta - \eta\nabla_\theta(\mathcal{L}_{awa} + \mathcal{L}_{ori})$
end
```

layers. Specifically, we first randomly select a target layer and then apply the awakening regularization term on the randomly sampled erased and disruptor filters within the target layer. Our main implementation is outlined in Algorithm 1. We also present the analysis in Section 4.3.1 to demonstrate that our EATS fosters equitable contributions among all filters across all layers.

3.3 Theoretical Proof in Awakening Inhibited Filters

In Section 3.2, we have introduced the training strategy that conceptualizes all filters within the network as active participants engaged in a collaborative game model. Its primary goal is to promote equitable contributions among all filters, ultimately enhancing overall generalization performance. Here, we leverage the Shapley value from the collaborative game theory to provide theoretical evidence, supporting the effectiveness of EATS in promoting equitable contributions among all filters.

For a fully convolutional neural network, $\mathcal{N}$, the Shapley value of the the i^{th} filter in the l^{th} layer, n_l^i, is represented as $\phi_{n_l^i}(\mathcal{M}, v)$, where $\mathcal{M}$ represents the sub-networks within the full network, *i.e.*, $\mathcal{M} \subseteq \mathcal{N}$. To facilitate the proof, we reformulate the Eq. 1 as follows:

$$\phi_{n_l^i}(\mathcal{M}, v) = \frac{1}{(|\mathcal{N}|-1)!} \sum_{\langle\mathcal{M}\rangle=|\mathcal{N}|-1} \frac{1}{|\mathcal{N}|} \sum_{\mathcal{S}\subset\mathcal{M}} [v(\mathcal{S} \cup \{n_l^i\}) - v(\mathcal{S})], \tag{5}$$

where $\langle\mathcal{M}\rangle = |\mathcal{N}|-1$ represents the set of ordered sequences of length $|\mathcal{N}|-1$ and $\mathcal{M}$ encompasses all consecutive subsequences of an ordered sequence starting from the first item, including the empty sequence. For example, if we have a set $\{A, B, C\}$, $|\mathcal{M}| = 3$ includes the ordered sequence such as $\{ABC, ACB, BAC, BCA, CAB, CBA\}$. For the sequence $\{ABC\}$, $\mathcal{M} = \{\emptyset, A, AB, ABC\}$, and for the sequence $\{BCA\}$, $\mathcal{M} = \{\emptyset, B, BC, BCA\}$.

We assume that the contribution of n_l^i decreases as the number of filters in l^{th} layer increases (*e.g.*, the contribution of A in $\{ABC\}$ is smaller than that in $\{AB\}$), we have:

$$\begin{aligned}
\phi_{n_l^i}(\mathcal{M}, v) &= \frac{1}{(|\mathcal{N}|-1)!} \sum_{\langle\mathcal{M}\rangle=|\mathcal{N}|-1} \frac{1}{|\mathcal{N}|} \sum_{\mathcal{S}\subset\mathcal{M}} [v(\mathcal{S} \cup \{n_l^i\}) - v(\mathcal{S})] \\
&\geq \frac{1}{(|\mathcal{N}|-1)!} \sum_{\langle\mathcal{M}\rangle=|\mathcal{N}|-1} \frac{1}{|\mathcal{N}|} \sum_{k=1}^{|\mathcal{N}|} [v(\mathcal{N}) - v(\mathcal{N}\backslash n_l^i)] \\
&\geq v(\mathcal{N}) - v(\mathcal{N}\backslash n_l^i),
\end{aligned} \tag{6}$$

where $\mathcal{N}$ corresponds to the original network f_θ and $\mathcal{N}\backslash n_l^i$ corresponds to the model after erasure $f_{\theta'}$. Recall that the awakening regularization term widens the performance gap between f_θ and $f_{\theta'}$ by effectively constraining the performance of $f_{\theta'}$. As a result, our EATS strategy plays a crucial role in awakening the cooperative relationship among all filters and fostering their equitable contributions to the prediction. While the theoretical proof underscores the fundamental effectiveness of our approach, we delve deeper into its effectiveness in improving generalization capability through extensive analyses, as detailed in Section 4.3.1.

4 EXPERIMENTS

4.1 EXPERIMENTAL SETTINGS

In the SR community, two predominant settings have gained widespread usage: the single-degradation setting (Timofte et al., 2017) and the multi-degradation setting (Wang et al., 2021; Zhang et al., 2021; Cao et al., 2023). We have opted for the second setting, where overfitting to a specific degradation scenario is no longer a viable option, and the primary challenge revolves around improving the generalization capacity of SR networks.

Following the configuration in Kong et al. (2022), we adopt the high-order degradation modelling (Wang et al., 2021) to conduct the multi-degradation setting. It involves sophisticated combinations of different degradations, including blur, downsampling, noise, and compression. Notably, these combinations are not applied singularly, but rather in multiple iterations to generate multi-faceted degradations. In addition, all factors (*e.g.*, kernels, downsampling scales, noise levels, and compression parameters) are subject to random sampling throughout the training process, where the hyper-parameters are identical to Wang et al. (2021); Kong et al. (2022).

We employ the high-quality images from the DIV2K (Agustsson & Timofte, 2017) dataset for training and the images from Set5 (Bevilacqua et al., 2012), Set14 (Yang et al., 2010), Manga109 (Matsui et al., 2017), Urban100 (Huang et al., 2015), and BSD100 (Martin et al., 2001) for testing. All models in this paper are implemented with PyTorch on NVIDIA GTX 3090 GPUs. We employ an Adam optimizer (Kingma & Ba, 2014) with $\beta_1 = 0.9$, $\beta_2 = 0.999$ to update our model with a batch of 16. The initial learning rate is set to 2×10^{-4} and subsequently modulated using the cosine annealing strategy. The patch size of the high-resolution is set to 128×128.

4.2 IMPLEMENTATION DETAILS

We select two representative SR networks, SRResNet Ledig et al. (2017) and RRDB Wang et al. (2018b), consistent with Kong et al. (2022), for our experimental investigations . To validate the efficacy of our erase-and-awaken training strategy, we create distinct variants of the baselines:

- Original: the baseline without any modifications;
- Dropout: incorporating the channel-wise dropout before the last convolution layer, where the drop probability is set to 0.5 and 0.7 for SRResNet and RRDB, respectively, according to the conclusion in Kong et al. (2022);
- EATS: training the baseline model with our Erase-and-Awaken Training Strategy (EATS).

For fair comparisons, we ensure that each competitive baseline and its variants undergo identical training configuration and optimization strategy.

4.3 COMPARISON AND ANALYSIS

4.3.1 ANALYSIS OF EATS

EATS encourages channels to contribute more equally to the prediction, alleviating the co-adapting problem. To provide further insight into the effectiveness of our EATS, we visualize the feature maps and channel salience maps (CSM) Kong et al. (2022). CSM is a gradient-based attribution analysis method that quantifies the contribution of each channel to the final result. In Fig. 3, we present the feature maps and corresponding CSMs for the output convolutional layer of both SRResNet and SRResNet-EATS. These visualizations demonstrate that integrating our training strategy can equalize the contributions of each channel to the prediction. This balanced contribution is crucial in improving the generalization capacity of the network.

EATS reduces correlations among channels. Our EATS randomly erases a filter in the SR network and constrains a performance drop for the erased network. This strategic approach aims to mitigate redundancy in the channel dimension while promoting feature diversity. To illustrate this effect, we conducted an analysis of channel correlations among both shallow and deep features, specifically focusing on the 2^{nd} and 14^{th} residual blocks of SRResNet and SRResNet-EATS. We utilize cosine similarity as a metric to measure the correlation of all paired channel responses within the same

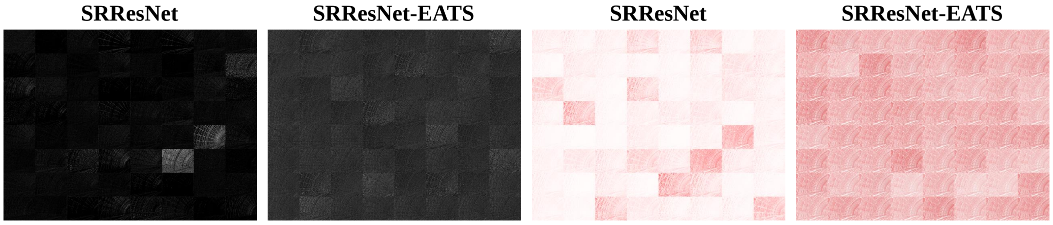

(a) Feature Map **(b) CSM**

Figure 3: The feature maps and CSM of SRResNet and SRResNet-EATS. It indicates that our EATS can promote the baseline to attain equatable channel responses and contributions to the prediction.

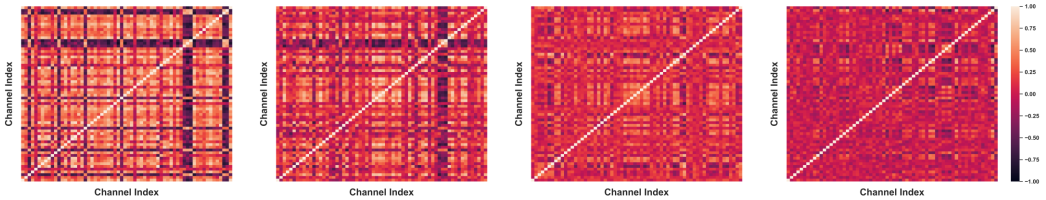

(a) 2^{nd} block of SRResNet **(b) 2^{nd} block of SRResNet-EATS** **(c) 14^{th} block of SRResNet** **(d) 14^{th} block of SRResNet-EATS**

Figure 4: Cosine similarity among channels of SRResNet and SRResNet-EATS. We select features from the 2^{nd} and 14^{th} residual blocks as the shallow and deep features. It indicates that integrating with our EATS reduces the correlation among feature channels and increases feature diversity.

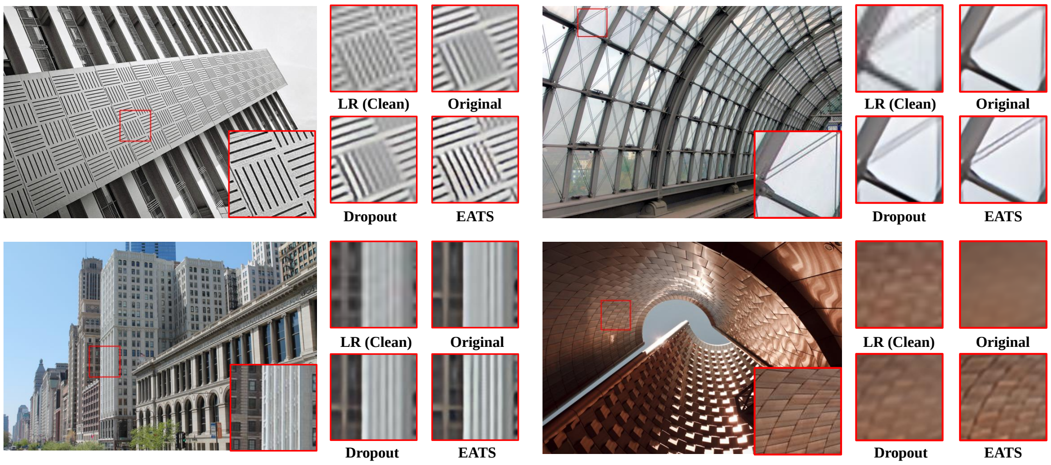

(a) SRResNet **(b) RRDBNet**

Figure 5: Visual comparison of SRResNet Ledig et al. (2017) and RRDBNet Wang et al. (2018b) on the Urban100 Huang et al. (2015) dataset.

layer. The visualization, as shown in Fig. 4 reveals that the channel responses of SRResNet exhibit a higher correlation, indicative of feature redundancy. In contrast, our EATS encourages the baseline to reduce the correlations in feature channels, thereby enhancing feature abundance.

4.3.2 Results on Multi-Degradation SR

To assess the generalization capacity, we create the complex degradations and their combinations using the high-quality images from the test sets through the data generation pipeline (Wang et al., 2021). Following Kong et al. (2022), we adopt Gaussian blur (kernel size 21 and standard deviation2, indicated by 'b'), bicubic downsampling, Gaussian noise (standard deviation 20, indicated by 'n'), and JPEG compression (quality 50, indicated by 'j') as the testing degradations. Furthermore, we generate complicated degradations formed through the combination of the above components.

Table 1: The PSNR results of SRResNet with ×4 downsampling scales. We apply bicubic, blur, noise, and jpeg to generate the degradation, *e.g.*, clean means only bicubic, b+n means blur → bicubic → noise. "Improvement" represents the performance difference between the SRResNet-EATS and the original SRResNet.

Config	Set5							
	clean	blur	noise	jpeg	b+n	b+j	n+j	b+n+j
Original	24.9697	24.6919	21.9275	23.7601	23.3022	23.4550	23.2996	22.9266
Dropout	25.6368	25.2455	21.9388	24.0995	23.4923	23.6830	23.5182	23.0791
EATS	25.7532	25.3635	22.0025	24.1728	23.5464	23.7347	23.5546	23.1193
Improvement	**+0.7835**	**+0.6716**	**+0.0750**	**+0.4127**	**+0.2442**	**+0.2797**	**+0.2550**	**+0.1927**
	Set14							
Original	22.6507	22.5816	20.7185	21.9326	21.9249	21.8599	21.7380	21.5619
Dropout	23.0847	22.9241	20.7914	22.1585	22.0182	22.0442	21.8873	21.6992
EATS	23.1282	22.9352	20.8249	22.2012	22.0533	22.0525	21.9293	21.7322
Improvement	**+0.4775**	**+0.3536**	**+0.1064**	**+0.2686**	**+0.1284**	**+0.1926**	**+0.1913**	**+0.1703**
	BSDS100							
Original	23.0997	23.0040	21.0617	22.5547	22.2802	22.4339	22.3151	22.1608
Dropout	23.4201	23.2857	21.1229	22.7574	22.3058	22.6000	22.4333	22.2425
EATS	23.4684	23.3306	21.1497	22.7820	22.3290	22.6195	22.4610	22.2602
Improvement	**+0.3687**	**+0.3266**	**+0.0880**	**+0.2273**	**+0.0488**	**+0.1856**	**+0.1459**	**+0.0994**
	Urban100							
Original	21.2966	21.0583	19.5806	20.7325	20.4667	20.4127	20.5519	20.1973
Dropout	21.6198	21.3153	19.6532	20.9153	20.5167	20.5494	20.6743	20.2759
EATS	21.6097	21.3348	19.6771	20.9109	20.5399	20.5525	20.6899	20.2883
Improvement	**+0.3131**	**+0.2765**	**+0.0965**	**+0.1784**	**+0.0732**	**+0.1398**	**+0.1380**	**+0.0910**
	Manga109							
Original	18.6740	18.9396	18.3484	18.4986	18.8332	18.7030	18.4797	18.6365
Dropout	19.0441	19.3156	18.4341	18.7711	19.0785	18.9471	18.7104	18.8350
EATS	19.0727	19.3203	18.4707	18.8026	19.0949	18.9529	18.7504	18.8522
Improvement	**+0.3987**	**+0.3807**	**+0.1223**	**+0.3040**	**+0.2617**	**+0.2499**	**+0.2707**	**+0.2157**

Tables 1 and 2 provide detailed quantitative evaluations of SRResNet and RRDBNet with distinct configurations across the various degradation conditions, demonstrating the effectiveness of our erase-and-awaken training strategy. Although dropout has undeniably enhanced the algorithm's generalization capability, our EATS exhibits remarkable potential for achieving even more substantial improvements. Comparing the results with the baseline model, we observe that EATS leads to remarkable improvements, with the maximum enhancement reaching 0.78 dB for SRResNet and an impressive 0.73 dB for RRDBNet. Furthermore, we compare EATS to dropout, the maximum gap extends to 0.12 dB for SRResNet and 0.21 dB for RRDB. In addition, visualizations in Fig. 5 provide qualitative evidence of EATS's effectiveness. By incorporating our EATS with the original baseline, the super-resolved images achieve more realistic content reconstruction and fine-grained textures without introducing artifacts.

5 Limitations

We will validate the effectiveness of the proposed training strategy on a broader spectrum of low-level tasks, including but not limited to image denoising and image deblurring. As a versatile training strategy, we encourage the exploration of various comprehensive networks integrated with our proposed approach. Our research goes beyond the design of a universal strategy for improving

Table 2: The PSNR results of RRDBNet with ×4 downsampling scale. We apply bicubic, blur, noise, and jpeg to generate the degradation, *e.g.*, clean means only bicubic, b+n means blur → bicubic → noise. "Improvement" represents the performance difference between the RRDBNet-EATS and the original RRDBNet.

Config	Set5							
	clean	blur	noise	jpeg	b+n	b+j	n+j	b+n+j
Original	25.2688	25.2776	22.2421	23.9881	23.3838	23.6890	23.4186	22.9922
Dropout	25.9292	25.5746	22.7143	24.3801	23.5175	23.9188	23.6084	23.1050
EATS	26.0074	25.7857	22.5926	24.4301	23.4469	23.8805	23.6479	23.0888
Improvement	**+0.7386**	**+0.5081**	**+0.3505**	**+0.4420**	**+0.0631**	**+0.1915**	**+0.2293**	**+0.0966**
	Set14							
Original	22.9262	22.8528	20.9357	22.1325	22.0795	21.9733	21.9026	21.6333
Dropout	23.2198	23.0626	21.0197	22.3072	22.2244	22.0923	22.0669	21.7556
EATS	23.4922	23.2615	21.2980	22.4989	22.1894	22.1938	22.1133	21.7674
Improvement	**+0.5660**	**+0.4087**	**+0.3623**	**+0.3664**	**+0.1099**	**+0.2205**	**+0.2107**	**+0.1341**
	BSDS100							
Original	23.3654	23.3880	21.2915	22.7456	22.3154	22.6020	22.4485	22.2281
Dropout	23.5886	23.5616	21.4746	22.8828	22.3895	22.7058	22.5420	22.2849
EATS	23.6963	23.6864	21.5848	22.9928	22.4043	22.7814	22.5743	22.3039
Improvement	**+0.3309**	**+0.2984**	**+0.2933**	**+0.2472**	**+0.0889**	**+0.1794**	**+0.1258**	**+0.0758**
	Urban100							
Original	21.5738	21.4637	19.5775	20.9649	20.4764	20.5970	20.7884	20.3406
Dropout	21.8104	21.6082	19.6290	21.1218	20.5096	20.6922	20.8822	20.3855
EATS	21.9979	21.6462	19.8111	21.2543	20.5088	20.7175	20.9688	20.4000
Improvement	**+0.4241**	**+0.1825**	**+0.2336**	**+0.2894**	**+0.0324**	**+0.1205**	**+0.1804**	**+0.0594**
	Manga109							
Original	18.6101	18.8597	18.4166	18.5256	19.0068	18.6980	18.5759	18.6658
Dropout	18.9249	19.0455	18.6042	18.7816	19.1874	18.8970	18.7588	18.7510
EATS	18.9220	19.0082	18.6622	18.8107	19.1926	18.9026	18.7213	18.7592
Improvement	**+0.3119**	**+0.1485**	**+0.2456**	**+0.2851**	**+0.1858**	**+0.2046**	**+0.1454**	**+0.0934**

the generalization performance of existing networks. It aims to introduce an alternative perspective, grounded in cooperative games within neural networks, for advancing generalization capacity. Therefore, our ongoing efforts will be dedicated to demonstrating the effectiveness of this approach across a wider range of computer vision tasks.

6 Conclusion

In this paper, we have introduced cooperative game theory to enhance the generalization capacity of image super-resolution algorithms in real-world scenarios, and proposed an Erase-and-Awaken Training Strategy (EATS). It treats all neurons within the network as active participants in a collaborative relationship, collectively determining the final prediction. Our EATS strategy effectively awakens previously suppressed neurons that hinder generalization and promotes equitable contributions among all neurons, thus alleviating effectively co-adaption problem and improving generalization performance. We provide theoretical proof of its effectiveness in promoting the contribution of each neuron to predictions. Notably, our approach can seamlessly integrate with existing networks, reinforcing their ability to generalize across unforeseen scenarios. Extensive experiments across various unseen datasets with distinct degradations consistently demonstrate the substantial performance gains achieved by incorporating our strategy.

REFERENCES

Eirikur Agustsson and Radu Timofte. NTIRE 2017 challenge on single image super-resolution: Dataset and study. In *Proceedings of the IEEE Conference on Computer Vision and Pattern Recognition Workshops*, pp. 126–135, 2017.

Marco Bevilacqua, Aline Roumy, Christine Guillemot, and Marie Line Alberi-Morel. Low-complexity single-image super-resolution based on nonnegative neighbor embedding. 2012.

Vladimir Bychkovsky, Sylvain Paris, Eric Chan, and Frédo Durand. Learning photographic global tonal adjustment with a database of input/output image pairs. In *Proceedings of the IEEE/CVF International Conference on Computer Vision*, pp. 97–104, 2011.

Jiezhang Cao, Qin Wang, Yongqin Xian, Yawei Li, Bingbing Ni, Zhiming Pi, Kai Zhang, Yulun Zhang, Radu Timofte, and Luc Van Gool. CiaoSR: Continuous implicit attention-in-attention network for arbitrary-scale image super-resolution. In *Proceedings of the IEEE/CVF Conference on Computer Vision and Pattern Recognition*, pp. 1796–1807, 2023.

Zheng Chen, Yulun Zhang, Jinjin Gu, Linghe Kong, Xin Yuan, et al. Cross aggregation transformer for image restoration. *Advances in Neural Information Processing Systems*, 35:25478–25490, 2022.

Tao Dai, Jianrui Cai, Yongbing Zhang, Shu-Tao Xia, and Lei Zhang. Second-order attention network for single image super-resolution. In *Proceedings of the IEEE/CVF conference on computer vision and pattern recognition*, pp. 11065–11074, 2019a.

Tao Dai, Jianrui Cai, Yongbing Zhang, Shu-Tao Xia, and Lei Zhang. Second-order attention network for single image super-resolution. In *Proceedings of the IEEE/CVF conference on computer vision and pattern recognition*, pp. 11065–11074, 2019b.

Chao Dong, Chen Change Loy, Kaiming He, and Xiaoou Tang. Learning a deep convolutional network for image super-resolution. In *Computer Vision–ECCV 2014: 13th European Conference, Zurich, Switzerland, September 6-12, 2014, Proceedings, Part IV 13*, pp. 184–199. Springer, 2014.

Chao Dong, Chen Change Loy, Kaiming He, and Xiaoou Tang. Image super-resolution using deep convolutional networks. *IEEE transactions on pattern analysis and machine intelligence*, 38(2): 295–307, 2015.

Jinjin Gu, Hannan Lu, Wangmeng Zuo, and Chao Dong. Blind super-resolution with iterative kernel correction. In *Proceedings of the IEEE/CVF Conference on Computer Vision and Pattern Recognition*, pp. 1604–1613, 2019.

Geoffrey E Hinton, Nitish Srivastava, Alex Krizhevsky, Ilya Sutskever, and Ruslan R Salakhutdinov. Improving neural networks by preventing co-adaptation of feature detectors. *arXiv preprint arXiv:1207.0580*, 2012.

Jia-Bin Huang, Abhishek Singh, and Narendra Ahuja. Single image super-resolution from transformed self-exemplars. In *Proceedings of the IEEE conference on computer vision and pattern recognition*, pp. 5197–5206, 2015.

Yan Huang, Shang Li, Liang Wang, Tieniu Tan, et al. Unfolding the alternating optimization for blind super resolution. *Advances in Neural Information Processing Systems*, 33:5632–5643, 2020.

Justin Johnson, Alexandre Alahi, and Li Fei-Fei. Perceptual losses for real-time style transfer and super-resolution. In *Computer Vision–ECCV 2016: 14th European Conference, Amsterdam, The Netherlands, October 11-14, 2016, Proceedings, Part II 14*, pp. 694–711. Springer, 2016.

Jiwon Kim, Jung Kwon Lee, and Kyoung Mu Lee. Accurate image super-resolution using very deep convolutional networks. In *Proceedings of the IEEE conference on computer vision and pattern recognition*, pp. 1646–1654, 2016.

Diederik P Kingma and Jimmy Ba. Adam: A method for stochastic optimization. *arXiv preprint arXiv:1412.6980*, 2014.

Xiangtao Kong, Xina Liu, Jinjin Gu, Yu Qiao, and Chao Dong. Reflash dropout in image super-resolution. In *Proceedings of the IEEE/CVF Conference on Computer Vision and Pattern Recognition*, pp. 6002–6012, 2022.

Wei-Sheng Lai, Jia-Bin Huang, Narendra Ahuja, and Ming-Hsuan Yang. Deep laplacian pyramid networks for fast and accurate super-resolution. In *Proceedings of the IEEE conference on computer vision and pattern recognition*, pp. 624–632, 2017.

Christian Ledig, Lucas Theis, Ferenc Huszár, Jose Caballero, Andrew Cunningham, Alejandro Acosta, Andrew Aitken, Alykhan Tejani, Johannes Totz, Zehan Wang, et al. Photo-realistic single image super-resolution using a generative adversarial network. In *Proceedings of the IEEE conference on computer vision and pattern recognition*, pp. 4681–4690, 2017.

Xin Li, Bingchen Li, Xin Jin, Cuiling Lan, and Zhibo Chen. Learning distortion invariant representation for image restoration from a causality perspective. In *Proceedings of the IEEE/CVF Conference on Computer Vision and Pattern Recognition*, pp. 1714–1724, 2023.

Bee Lim, Sanghyun Son, Heewon Kim, Seungjun Nah, and Kyoung Mu Lee. Enhanced deep residual networks for single image super-resolution. In *Proceedings of the IEEE conference on computer vision and pattern recognition workshops*, pp. 136–144, 2017.

Jie Liu, Wenjie Zhang, Yuting Tang, Jie Tang, and Gangshan Wu. Residual feature aggregation network for image super-resolution. In *Proceedings of the IEEE/CVF conference on computer vision and pattern recognition*, pp. 2359–2368, 2020.

Yihao Liu, Anran Liu, Jinjin Gu, Zhipeng Zhang, Wenhao Wu, Yu Qiao, and Chao Dong. Discovering distinctive" semantics" in super-resolution networks. *arXiv preprint arXiv:2108.00406*, 2021.

Yihao Liu, Hengyuan Zhao, Jinjin Gu, Yu Qiao, and Chao Dong. Evaluating the generalization ability of super-resolution networks. *arXiv preprint arXiv:2205.07019*, 2022.

Cheng Ma, Yongming Rao, Yean Cheng, Ce Chen, Jiwen Lu, and Jie Zhou. Structure-preserving super resolution with gradient guidance. In *Proceedings of the IEEE/CVF conference on computer vision and pattern recognition*, pp. 7769–7778, 2020.

Salma Abdel Magid, Yulun Zhang, Donglai Wei, Won-Dong Jang, Zudi Lin, Yun Fu, and Hanspeter Pfister. Dynamic high-pass filtering and multi-spectral attention for image super-resolution. In *Proceedings of the IEEE/CVF International Conference on Computer Vision*, pp. 4288–4297, 2021.

David Martin, Charless Fowlkes, Doron Tal, and Jitendra Malik. A database of human segmented natural images and its application to evaluating segmentation algorithms and measuring ecological statistics. In *Proceedings Eighth IEEE International Conference on Computer Vision. ICCV 2001*, volume 2, pp. 416–423. IEEE, 2001.

Yusuke Matsui, Kota Ito, Yuji Aramaki, Azuma Fujimoto, Toru Ogawa, Toshihiko Yamasaki, and Kiyoharu Aizawa. Sketch-based manga retrieval using manga109 dataset. *Multimedia Tools and Applications*, 76:21811–21838, 2017.

Ben Niu, Weilei Wen, Wenqi Ren, Xiangde Zhang, Lianping Yang, Shuzhen Wang, Kaihao Zhang, Xiaochun Cao, and Haifeng Shen. Single image super-resolution via a holistic attention network. In *Computer Vision–ECCV 2020: 16th European Conference, Glasgow, UK, August 23–28, 2020, Proceedings, Part XII 16*, pp. 191–207. Springer, 2020.

Mehdi SM Sajjadi, Bernhard Scholkopf, and Michael Hirsch. Enhancenet: Single image super-resolution through automated texture synthesis. In *Proceedings of the IEEE international conference on computer vision*, pp. 4491–4500, 2017.

Radu Timofte, Eirikur Agustsson, Luc Van Gool, Ming-Hsuan Yang, and Lei Zhang. NTIRE 2017 challenge on single image super-resolution: Methods and results. In *Proceedings of the IEEE conference on computer vision and pattern recognition workshops*, pp. 114–125, 2017.

Jiamian Wang, Huan Wang, Yulun Zhang, Yun Fu, and Zhiqiang Tao. Iterative soft shrinkage learning for efficient image super-resolution. *arXiv preprint arXiv:2303.09650*, 2023.

Xintao Wang, Ke Yu, Chao Dong, and Chen Change Loy. Recovering realistic texture in image super-resolution by deep spatial feature transform. In *Proceedings of the IEEE Conference on Computer Vision and Pattern Recognition*, pp. 606–615, 2018a.

Xintao Wang, Ke Yu, Shixiang Wu, Jinjin Gu, Yihao Liu, Chao Dong, Yu Qiao, and Chen Change Loy. ESRGAN: Enhanced super-resolution generative adversarial networks. In *Proceedings of the European conference on computer vision (ECCV) workshops*, pp. 0–0, 2018b.

Xintao Wang, Liangbin Xie, Chao Dong, and Ying Shan. Real-ESRGAN: Training real-world blind super-resolution with pure synthetic data. In *Proceedings of the IEEE/CVF international conference on computer vision*, pp. 1905–1914, 2021.

Bin Xia, Yucheng Hang, Yapeng Tian, Wenming Yang, Qingmin Liao, and Jie Zhou. Efficient non-local contrastive attention for image super-resolution. In *Proceedings of the AAAI Conference on Artificial Intelligence*, volume 36, pp. 2759–2767, 2022.

Jianchao Yang, John Wright, Thomas S Huang, and Yi Ma. Image super-resolution via sparse representation. *IEEE transactions on image processing*, 19(11):2861–2873, 2010.

Yuan Yuan, Siyuan Liu, Jiawei Zhang, Yongbing Zhang, Chao Dong, and Liang Lin. Unsupervised image super-resolution using cycle-in-cycle generative adversarial networks. In *Proceedings of the IEEE conference on computer vision and pattern recognition workshops*, pp. 701–710, 2018.

Jiale Zhang, Yulun Zhang, Jinjin Gu, Yongbing Zhang, Linghe Kong, and Xin Yuan. Accurate image restoration with attention retractable transformer. *arXiv preprint arXiv:2210.01427*, 2022.

Kai Zhang, Wangmeng Zuo, and Lei Zhang. Learning a single convolutional super-resolution network for multiple degradations. In *Proceedings of the IEEE conference on computer vision and pattern recognition*, pp. 3262–3271, 2018a.

Kai Zhang, Jingyun Liang, Luc Van Gool, and Radu Timofte. Designing a practical degradation model for deep blind image super-resolution. In *Proceedings of the IEEE/CVF International Conference on Computer Vision*, pp. 4791–4800, 2021.

Yulun Zhang, Kunpeng Li, Kai Li, Lichen Wang, Bineng Zhong, and Yun Fu. Image super-resolution using very deep residual channel attention networks. In *Proceedings of the European Conference on Computer Vision (ECCV)*, pp. 286–301, 2018b.

Yulun Zhang, Kunpeng Li, Kai Li, Bineng Zhong, and Yun Fu. Residual non-local attention networks for image restoration. *arXiv preprint arXiv:1903.10082*, 2019.

Shangchen Zhou, Jiawei Zhang, Wangmeng Zuo, and Chen Change Loy. Cross-scale internal graph neural network for image super-resolution. *Advances in neural information processing systems*, 33:3499–3509, 2020.

Anqi Zhu, Lin Zhang, Ying Shen, Yong Ma, Shengjie Zhao, and Yicong Zhou. Zero-shot restoration of underexposed images via robust Retinex decomposition. In *Proceedings of the IEEE International Conference on Multimedia and Expo*, pp. 1–6, 2020.

APPENDIX

- We further evaluate the effectiveness of our EATS on super-resolution with ×2 scaling.
- We evaluate the effectiveness of our EATS on another attention-based algorithm.
- We discuss the training costs incurred by our proposed EATS.
- We validate the convergence of the awakening regularization in our EATS.
- We conduct the ablation studies to investigate the impact of varying layer ratios in the erase-and-awaken training strategy on SRResNet.
- We conduct the ablation studies to investigate the impact of the number of involved filters in each training iteration on SRResNet.
- We analyze the effectiveness of our EATS on reducing correlations among channels on more layers within SRResNet and RRDBNet.
- We analyze the effectiveness of our EATS on alleviating co-adaption phenomenon in both shallow and deep layers.
- We present more visualization results on different degradation configurations.

A GENERALIZATION PERFORMANCE ON X2 SCALING

Tab. 3 and 4 provide quantitative evaluations of SRResNet and RRDBNet on ×2 scaling, which further demonstrates the effectiveness of our erase-and-awaken training strategy. Comparing the results with the baseline model, we observe that EATS leads to remarkable improvements, with the maximum enhancement reaching 0.53 dB for SRResNet and an impressive 0.66 dB for RRDBNet. Furthermore, we comare EATS to dropout, the maximum gap extends to 0.15 dB for SRResNet and 0.12 dB for RRDB.

Table 3: The PSNR results of SRResNet with ×2. We apply bicubic, blur, noise and jpeg to generate the degradation, *e.g.*, clean means only bicubic, b+n means blur → bicubic → noise. "Improvement" represents that the performance enhancement of SRResNet-EATS compared to the SRResNet.

Config	Set5							
	clean	blur	noise	jpeg	b+n	b+j	n+j	b+n+j
Original	26.8084	26.8084	24.1133	26.8350	25.0767	25.8566	26.1467	24.9306
Dropout	27.2030	27.2030	24.2231	27.1348	25.1975	26.1130	26.4176	25.1576
EATS	27.3422	27.3422	24.2282	27.1906	25.2221	26.1967	26.4641	25.1835
Improvement	**+0.5338**	**+0.5338**	**+0.1149**	**+0.3556**	**+0.1454**	**+0.3401**	**+0.3174**	**+0.2529**
Set14								
Original	25.7810	24.7398	22.8671	24.9982	23.5337	23.9898	24.5282	23.4352
Dropout	26.0030	24.8413	22.9801	25.1041	23.5441	24.0763	24.6533	23.5380
EATS	26.0541	24.9154	22.9606	25.1198	23.5664	24.1157	24.6745	23.5584
Improvement	**+0.2731**	**+0.1756**	**+0.0935**	**+0.1216**	**+0.0327**	**+0.1259**	**+0.1463**	**+0.1232**
BSDS100								
Original	25.4314	24.6299	22.6302	24.8488	23.4511	24.1568	24.4636	23.6270
Dropout	25.5721	24.7310	22.7676	24.9370	23.5241	24.2373	24.5331	23.7019
EATS	25.5592	24.7149	22.7614	24.9195	23.5120	24.2211	24.5331	23.6943
Improvement	**+0.1278**	**+0.0850**	**+0.1312**	**+0.0707**	**+0.0609**	**+0.0643**	**+0.0695**	**+0.0673**
Urban100								
Original	24.1966	22.6617	21.7665	23.4633	21.7126	22.0602	23.1523	21.6205
Dropout	24.4202	22.7573	21.8302	23.6326	21.7265	22.1770	23.3069	21.7268
EATS	24.4522	22.8045	21.8139	23.6467	21.7413	22.2080	23.3266	21.7425
Improvement	**+0.2556**	**+0.1428**	**+0.0474**	**+0.1834**	**+0.0287**	**+0.1478**	**+0.1743**	**+0.1220**
Manga100								
Original	25.4198	24.6002	23.2008	24.6422	23.4303	23.7406	24.3533	23.1404
Dropout	25.9607	24.7978	23.3060	24.9350	23.5122	23.8499	24.6198	23.2815
EATS	25.9105	24.8264	23.2846	24.9009	23.5090	23.8747	24.6052	23.2811
Improvement	**+0.4907**	**+0.2262**	**+0.0838**	**+0.2587**	**+0.0787**	**+0.1341**	**+0.2519**	**+0.1407**

Table 4: The PSNR results of RRDBNet with ×2. We apply bicubic, blur, noise and jpeg to generate the degradation, *e.g.*, clean means only bicubic, b+n means blur → bicubic → noise. "Improvement" represents that the performance enhancement of RRDBNet-EATS compared to the RRDBNet.

Config	Set5							
	clean	blur	noise	jpeg	b+n	b+j	n+j	b+n+j
Original	28.1476	27.3172	25.2403	27.1145	24.4877	26.1389	26.4795	25.2270
Dropout	28.7062	28.1439	25.5222	27.4045	25.9662	26.5147	26.7263	25.5055
EATS	28.8104	28.2165	25.6271	27.5202	25.9556	26.5562	26.7342	25.4417
Improvement	**+0.6628**	**+0.8993**	**+0.3868**	**+0.4057**	**+1.4679**	**+0.4173**	**+0.2547**	**+0.2147**
Set14								
Original	24.7354	24.2766	23.1168	24.2496	23.1845	23.5462	23.8335	22.9599
Dropout	24.9120	24.5681	23.2643	24.3428	23.3876	23.7963	23.9163	23.1106
EATS	24.9919	24.5677	23.3152	24.4157	23.3765	23.7612	23.9477	23.0522
Improvement	**+0.2565**	**+0.2911**	**+0.1984**	**+0.1661**	**+0.1920**	**+0.2150**	**+0.1142**	**+0.0923**
BSDS100								
Original	24.4175	24.2773	23.1084	24.0722	23.3309	23.7638	23.4950	23.2252
Dropout	24.5992	24.4672	23.2565	24.1994	23.4885	23.8946	23.8661	23.3335
EATS	24.5628	24.4898	23.2679	24.1741	23.4937	23.8912	23.8320	23.3250
Improvement	**+0.1453**	**+0.2125**	**+0.1595**	**+0.1019**	**+0.1628**	**+0.1274**	**+0.3370**	**+0.0998**
Urban100								
Original	24.3659	23.1373	22.5218	23.7493	21.9898	22.4042	23.3622	21.8094
Dropout	24.6209	23.3539	22.6854	23.9605	22.1361	22.5125	23.5329	21.9296
EATS	24.5982	23.4233	22.7519	23.9508	22.1754	22.5445	23.5341	21.9513
Improvement	**+0.2323**	**+0.2860**	**+0.2301**	**+0.2015**	**+0.1856**	**0.1403**	**+0.1719**	**+0.1419**
Manga100								
Original	19.6360	20.2221	19.9389	19.6657	20.3215	20.1687	19.7929	20.2302
Dropout	19.7362	20.5398	20.0121	19.7291	20.5115	20.4014	19.8055	20.3722
EATS	19.7097	20.4536	20.0801	19.7278	20.4450	20.3553	19.8096	20.3086
Improvement	**+0.0737**	**+0.2315**	**+0.1412**	**+0.0621**	**+0.1235**	**+0.1866**	**+0.0167**	**+0.0784**

B PERFORMANCE ON ATTENTION-BASED APPROACH

we have evaluated the effectiveness of our proposed EATS using a lightweight variant of HAN Niu et al. (2020) with x4 scaling. This lightweight version comprises approximately 1/20 of the parameters found in the original network. To maintain consistency with the experimental settings outlined in the manuscript, we have re-trained both the lightweight HAN and HAN-EATS, incorporating high-order degradation modeling. The quantitative results are presented in Table 5.

Table 5: The PSNR results of HAN with ×4. We apply bicubic, blur, noise and jpeg to generate the degradation, *e.g.*, clean means only bicubic, b+n means blur → bicubic → noise. "Improvement" represents that the performance enhancement of HAN-EATS compared to the HAN.

Config	Set5							
	clean	blur	noise	jpeg	b+n	b+j	n+j	b+n+j
Original	25.4834	25.4207	22.5964	24.1479	23.7007	23.8615	23.5668	23.1275
EATS	26.1176	25.8898	22.8330	24.4354	23.8923	23.9615	23.6703	23.1699
Improvement	**0.6342**	**0.4691**	**0.2366**	**0.2875**	**0.1916**	**0.1000**	**0.1035**	**0.0424**
	Set14							
Original	23.0610	23.1144	21.3902	22.2880	22.3199	22.2746	22.0212	21.7860
EATS	23.4764	23.3560	21.5058	22.4861	22.3971	22.2772	22.1089	21.7872
Improvement	**0.4154**	**0.2416**	**0.1156**	**0.1981**	**0.0772**	**0.0026**	**0.0877**	**0.0012**
	BSDS100							
Original	23.4619	23.4352	21.7799	22.8227	22.5801	22.7466	22.4817	22.2781
EATS	23.6903	23.5756	21.8599	22.9232	22.6394	22.7573	22.5339	22.2937
Improvement	**0.2284**	**0.1404**	**0.0800**	**0.1005**	**0.0593**	**0.0107**	**0.0522**	**0.0156**
	Urban100							
Original	21.6242	21.5168	20.2169	21.0329	20.7608	20.7810	20.7895	20.3836
EATS	21.9152	21.7400	20.2708	21.1839	20.7677	20.8224	20.8381	20.3987
Improvement	**0.2910**	**0.2232**	**0.0539**	**0.1510**	**0.0069**	**0.0414**	**0.0486**	**0.0151**
	Manga100							
Original	18.9412	19.2265	18.6995	18.7634	19.1281	19.0087	18.7372	18.7624
EATS	19.3123	19.5149	18.8154	19.0205	19.2600	19.1412	18.8486	18.9039
Improvement	**0.3711**	**0.2884**	**0.1159**	**0.2571**	**0.1319**	**0.1325**	**0.1114**	**0.1415**

C Training costs incurred by our EATS

Firstly, it's essential to emphasize that our proposed Erasing and Awakening Training Scheme (EATS) does not introduce additional training parameters. Within a training iteration, we conduct a forward propagation of the original network, f_θ, calculating the original loss function, $\mathcal{L}_{ori}$. Subsequently, our EATS involves randomly replacing an erased filter with a disrupted filter based on the original network, resulting in a modified network after erasure, $f_{\theta'}$). We then calculate the awakening regularization, $\mathcal{L}_{awa}$, through a second forward propagation. The network is update based on the combination of these two loss functions. Therefore, it's crucial to note that our EATS only requires two forward propagations, as opposed to employing two separate neural networks.

Secondly, the two forward propagations in our training paradigm marginally increase training times, approximately by 1.4 times compared to the corresponding original networks. This increment is deemed acceptable, especially considering the significant improvement in generalization capability.

Lastly, it's important to highlight that our training paradigm is exclusively applied during the training process and does not impose any additional computational burden during the inference phase.

D Convergence of the awakening regularization

We present the visualizations of the original loss, $\mathcal{L}_{ori}$, and our awakening regularization, $\mathcal{L}_{awa}$, during the training process of SRResNet-EATS and RRDBNet-EATS. Through the plots presented in Fig. 6, it is evident that the awakening regularization progressively decreases and converges with the training iteration.

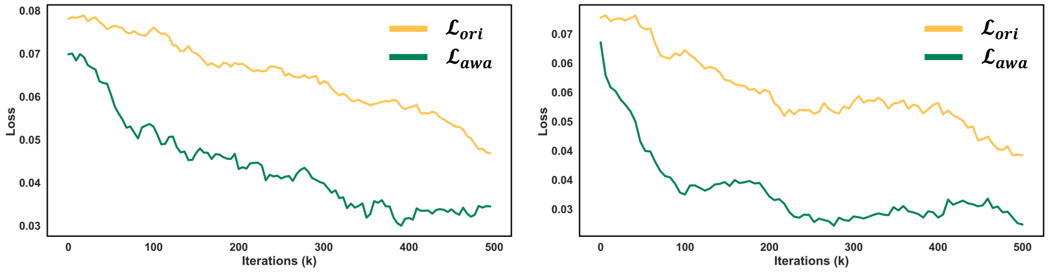

(a) SRResNet-EATS

(b) RRDBNet-EATS

Figure 6: The curves of the original loss and the awakening regularization of SRResNet-EATS and RRDBNet-EATS during the training process..

E Ablation Studies about the ration of involved layers

Table 6: Ablation studies about the impact of varying layer ratios involved in the erase-and-awaken training strategy on RRDBNet with × 4 scaling. We apply bicubic, blur, noise and jpeg to generate the degradation, *e.g.*, clean means only bicubic, b+n means blur → bicubic → noise.

Config	Set5							
	clean	blur	noise	jpeg	b+n	b+j	n+j	b+n+j
Original	25.2688	25.2776	22.2421	23.9881	23.3838	23.6890	23.4186	22.9922
EATS-20%	25.4705	25.4355	22.0787	24.0810	23.5124	23.7079	23.4250	22.9718
EATS-40%	25.6724	25.7932	22.1805	24.2320	23.6813	23.8129	23.5765	23.0717
EATS-60%	25.7675	25.7484	22.3898	24.2352	23.3675	23.8208	23.5615	23.0379
EATS-80%	25.8453	25.9380	22.4460	24.2615	23.5560	23.8024	23.5686	22.9833
EATS	26.0074	25.7857	22.5926	24.4301	23.4469	23.8805	23.6479	23.0888
Set14								
Original	22.9262	22.8528	20.9357	22.1325	22.0795	21.9733	21.9026	21.6333
EATS-20%	23.0829	23.0253	21.0489	22.2179	22.2532	22.0621	21.9563	21.6807
EATS-40%	23.2977	23.2232	21.1205	22.3883	22.3323	22.1927	22.0753	21.7727
EATS-60%	23.3332	23.2649	21.2404	22.3337	22.1578	22.1454	22.0184	21.7227
EATS-80%	23.3325	23.2644	21.2415	22.3583	22.2633	22.1002	22.0565	21.5745
EATS	23.4922	23.2615	21.2980	22.4989	22.1894	22.1938	22.1133	21.7674
BSDS100								
Original	23.3654	23.3880	21.2915	22.7456	22.3154	22.6020	22.4485	22.2281
EATS-20%	23.4795	23.5016	21.3462	22.8051	22.4628	22.6454	22.4641	22.2288
EATS-40%	23.5306	23.5857	21.4433	22.8932	22.5713	22.7332	22.5348	22.2917
EATS-60%	23.6355	23.6796	21.4363	22.9088	22.3937	22.7411	22.5395	22.2907
EATS-80%	23.6380	23.7344	21.5845	22.9338	22.5199	22.7489	22.5507	22.2736
EATS	23.6963	23.6864	21.5848	22.9928	22.4043	22.7814	22.5743	22.3039
Urban100								
Original	21.5738	21.4637	19.5775	20.9649	20.4764	20.5970	20.7884	20.3406
EATS-20%	21.7343	21.5404	19.6680	21.0606	20.5837	20.6305	20.8302	20.3423
EATS-40%	21.7314	21.6119	19.7038	21.0855	20.6532	20.6820	20.8592	20.3655
EATS-60%	21.8647	21.7017	19.7688	21.1319	20.5048	20.6927	20.8826	20.3864
EATS-80%	21.9305	21.7670	19.7500	21.1860	20.6358	20.6939	20.9345	20.3794
EATS	21.9979	21.6462	19.8111	21.2543	20.5088	20.7175	20.9688	20.4000
Manga100								
Original	18.6101	18.8597	18.4166	18.5256	19.0068	18.6980	18.5759	18.6658
EATS-20%	18.7687	18.9854	18.5131	18.6210	19.1806	18.7449	18.6311	18.7002
EATS-40%	18.7363	18.9413	18.5269	18.6576	19.2270	18.8488	18.6335	18.7278
EATS-60%	18.7884	19.0606	18.5614	18.6790	19.2359	18.8396	18.6443	18.7303
EATS-80%	18.7912	18.9745	18.6295	18.6941	19.2364	18.8263	18.6835	18.7262
EATS	19.9220	19.0082	18.6622	18.8107	19.1926	18.9026	18.7213	18.7592

F Ablation Studies about the number of involved filters in each training iteration

Our experiments explored configurations with 1 (default), 3, and 5 filters engaged in each iteration. Compared to the default of 1 filter, involving 3 filters achieved only a slight improvement. This decline may be attributed to increased randomness and instability during the training process.

Table 7: Ablation studies about the number of involved filters in each training iteration on RRDBNet with × 4 scaling. We apply bicubic, blur, noise and jpeg to generate the degradation, *e.g.*, clean means only bicubic, b+n means blur → bicubic → noise.

Config	Set5							
	clean	blur	noise	jpeg	b+n	b+j	n+j	b+n+j
Original	25.2688	25.2776	22.2421	23.9881	23.3838	23.6890	23.4186	22.9922
EATS-1filter (default)	26.0074	25.7857	22.5926	24.4301	23.4469	23.8805	23.6479	23.0888
EATS-3filter	26.0538	25.9900	22.5482	24.4395	23.6294	23.9155	23.5702	23.0095
EATS-5filter	25.8929	25.6534	22.4461	24.2632	23.5130	23.8032	23.5774	23.0124
Set14								
Original	22.9262	22.8528	20.9357	22.1325	22.0795	21.9733	21.9026	21.6333
EATS-1filter (default)	23.4922	23.2615	21.2980	22.4989	22.1894	22.1938	22.1133	21.7674
EATS-3filter	23.6219	23.3394	21.3617	22.5045	22.3048	22.1650	22.0960	21.7275
EATS-5filter	23.4872	23.1491	21.2607	22.4014	22.0382	22.1274	22.0476	21.7356
BSDS100								
Original	23.3654	23.3880	21.2915	22.7456	22.3154	22.6020	22.4485	22.2281
EATS-1filter (default)	23.6963	23.6864	21.5848	22.9928	22.4043	22.7814	22.5743	22.3039
EATS-3filter	23.7743	23.7075	21.7250	23.0244	22.5536	22.8058	22.5950	22.3234
EATS-5filter	23.5557	23.5699	21.4584	22.9784	22.5033	22.7022	22.5667	22.3020
Urban100								
Original	21.5738	21.4637	19.5775	20.9649	20.4764	20.5970	20.7884	20.3406
EATS-1filter (default)	21.9979	21.6462	19.8111	21.2543	20.5088	20.7175	20.9688	20.4000
EATS-3filter	21.9795	21.7051	19.9301	21.2136	20.6727	20.6532	20.9733	20.3649
EATS-5filter	21.8009	21.5756	19.7940	21.1980	20.4379	20.6861	20.9068	20.3656
Manga100								
Original	18.6101	18.8597	18.4166	18.5256	19.0068	18.6980	18.5759	18.6658
EATS-1filter (default)	19.9220	19.0082	18.6622	18.8107	19.1926	18.9026	18.7213	18.7592
EATS-3filter	19.9446	19.2506	18.8891	18.8846	19.2921	19.9487	18.7675	18.7990
EATS-5filter	19.8026	18.9324	18.6103	18.8145	19.1652	18.8039	18.7179	18.7605

G More Visualizations about the Feature Correlations

We visualize more channel correlation matrix on 2^{nd}, 8^{th}, 14^{th} and output layer wihtin the SRResNet and RRDBNet in Fig. 7 and Fig. 8, respectively. We utilize cosine similarity as a metric to measure the correlation of all paired channel responses within the same layer. The visualization reveals that the channel responses of baseline models exhibit higher correlation, indicative of feature redundancy. In contrast, our EATS encourages the baselines to reduce the correlations in feature channels, thereby enhancing feature abundance.

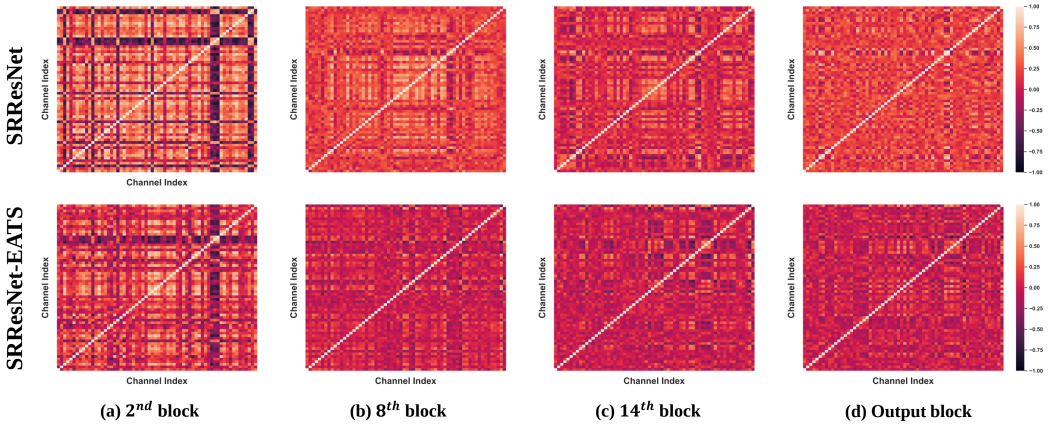

(a) 2^{nd} block (b) 8^{th} block (c) 14^{th} block (d) Output block

Figure 7: Cosine similarity among channels of SRResNet and SRResNet-EATS. We select features from the 2^{nd}, 8^{th}, 14^{th} and output blocks as the shallow and deep features. It indicates that integrating with our EATS reduces the correlation among feature channels and increases feature diversity.

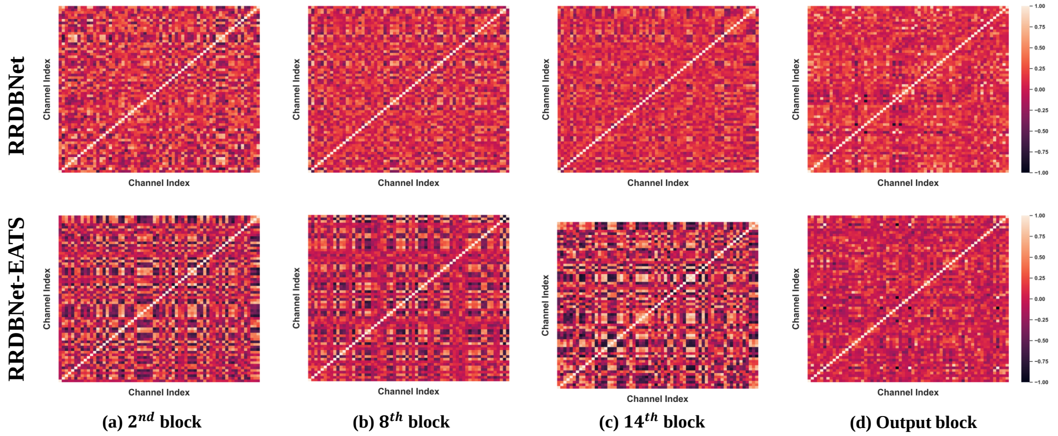

(a) 2^{nd} block (b) 8^{th} block (c) 14^{th} block (d) Output block

Figure 8: Cosine similarity among channels of RRDBNet and RRDBNet-EATS. We select features from the 2^{nd}, 8^{th}, 14^{th} and output blocks as the shallow and deep features. It indicates that integrating with our EATS reduces the correlation among feature channels and increases feature diversity.

H ALLEVIATING CO-ADAPTION IN BOTH SHALLOW AND DEEP LAYERS.

The conclusions draw from the previous work Kong et al. (2022) indicates that employing dropout only at the last convolutional layer improves generalization performance, while even causing drop in performance at other layers. Therefore, we conducted a statistical analysis of channel responses in the 2^{nd} and last output layers of SRResNet Ledig et al. (2017), SRResNet with dropout, and SRResNet-EATS (all trained on the Five5K Bychkovsky et al. (2011) dataset) across 100 randomly sampled unseen images. The results, as shown in Fig. 9, indicate that while dropout operation can alleviate the co-adaptation Hinton et al. (2012) phenomenon in the last layer, it fails to address the issue in the shallow layers. In contrast, incorporating our training strategy effectively mitigates co-adaptation and achieves equitable channel responses in both shallow and deep layers.

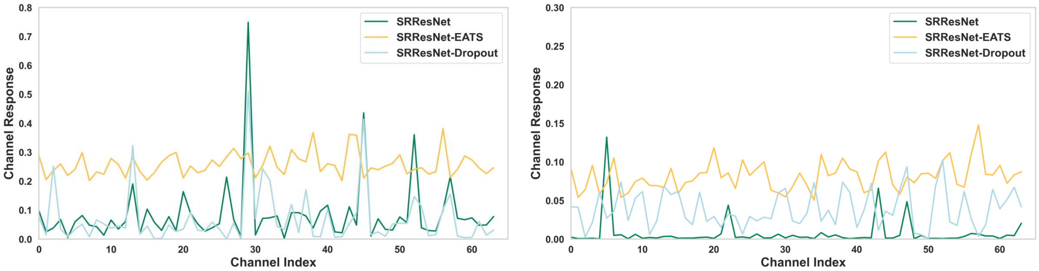

(a) 2^{nd} block **(b) Output block**

Figure 9: The Erase-and-Awaken Training Strategy (EATS) mitigates the co-adaption problem in both shallow and deep layers, 2^{th} and output block. We analyze channel responses in unseen scenarios, averaging channel responses from the 2^{nd} block in SRResNet (trained on Five5K) across 100 randomly sampled unseen images. It reveals the co-adaption phenomenon (Hinton et al., 2012), where a few channels are highly activated while others are inhibited. As the dropout operation is strategically applied (only the output layer) Kong et al. (2022), its effectiveness is limited to mitigating co-adaptation in deeper layers. Conversely, the integration of EATS with SRResNet yields balanced and activated channel responses in both shallow and deep layers.

I More Visualizations

In this section, we provide additional qualitative results on different degradations to show the effectiveness of our EATS (see Fig. 10 to Fig.17). Following consistent configurations with the manuscript, we adopt Gaussian blur (kernel size 21 and standard deviation2, indicated by ”b”), bicubic downsampling, Gaussian noise (standard deviation 20, indicated by ”n”), and JPEG compression (quality 50, indicated by ”j”) as the testing degradations. In addition to the single degradation, we synthesize the complicated mixed degradations with the second degradation process Wang et al. (2021).

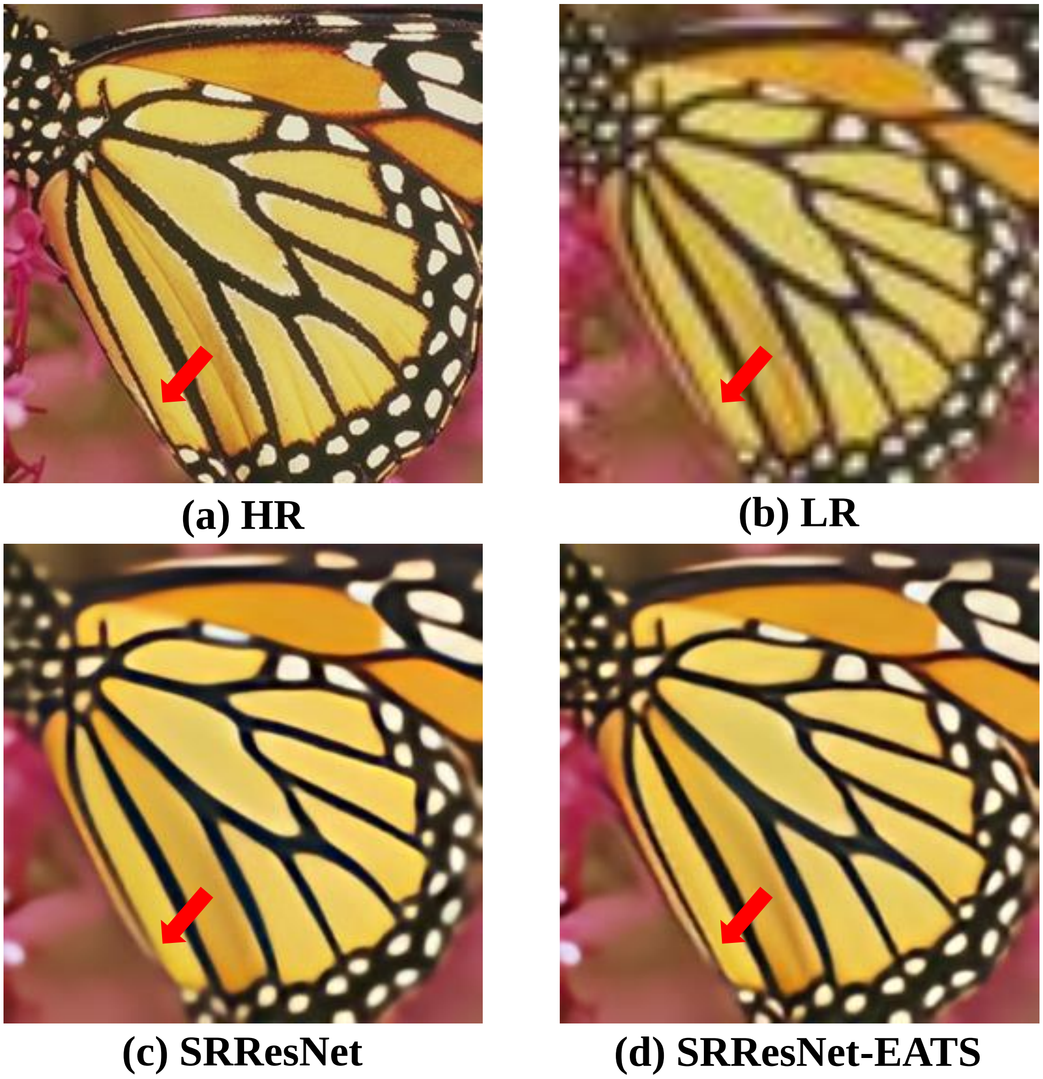

Figure 10: Visual comparison of SRResNet Ledig et al. (2017) on the clean-Set5 Bevilacqua et al. (2012).

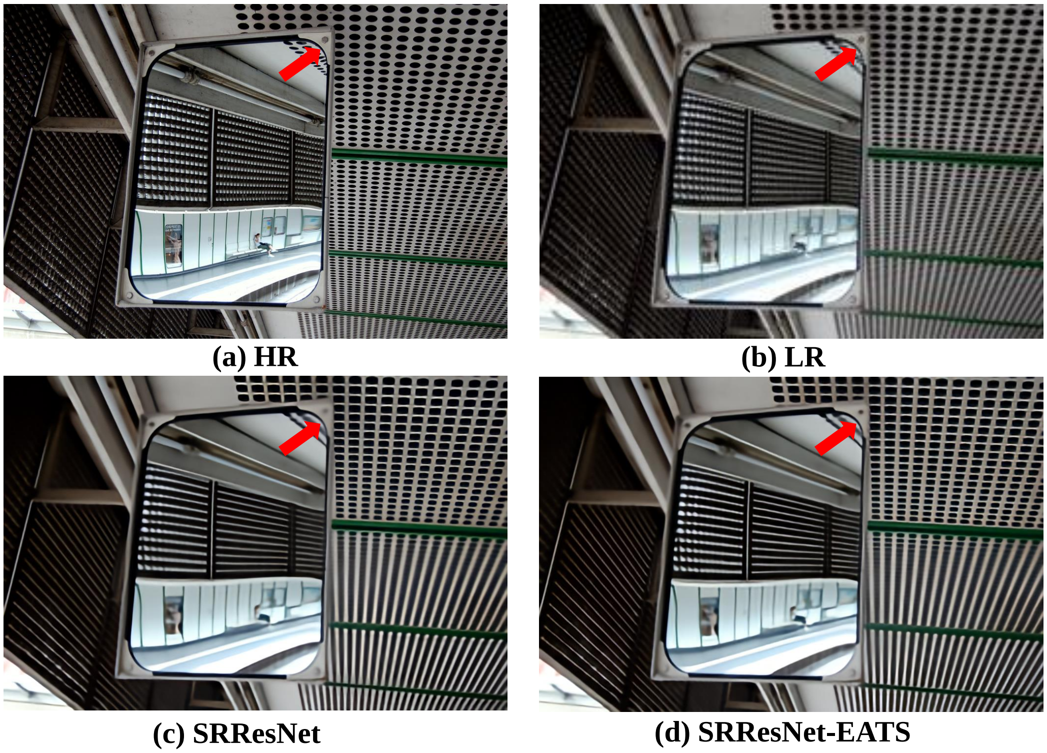

Figure 11: Visual comparison of SRResNet Ledig et al. (2017) on the blur-Urban100 Huang et al. (2015).

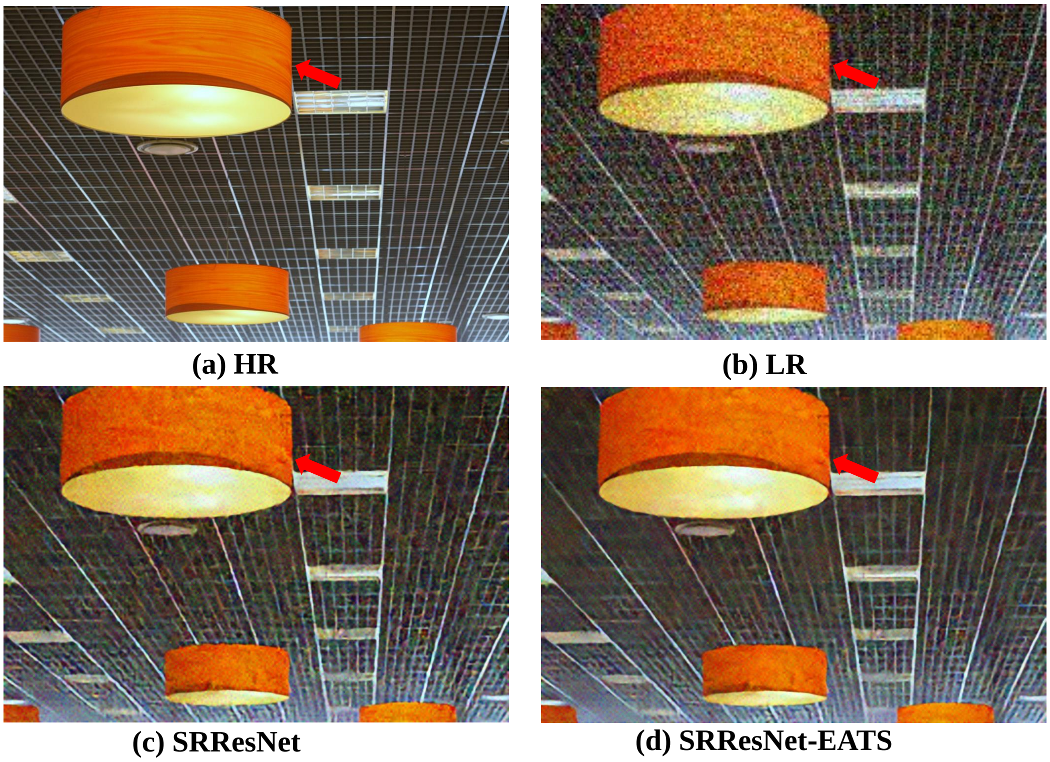

Figure 12: Visual comparison of SRResNet Ledig et al. (2017) on the noise-Urban100 Huang et al. (2015).

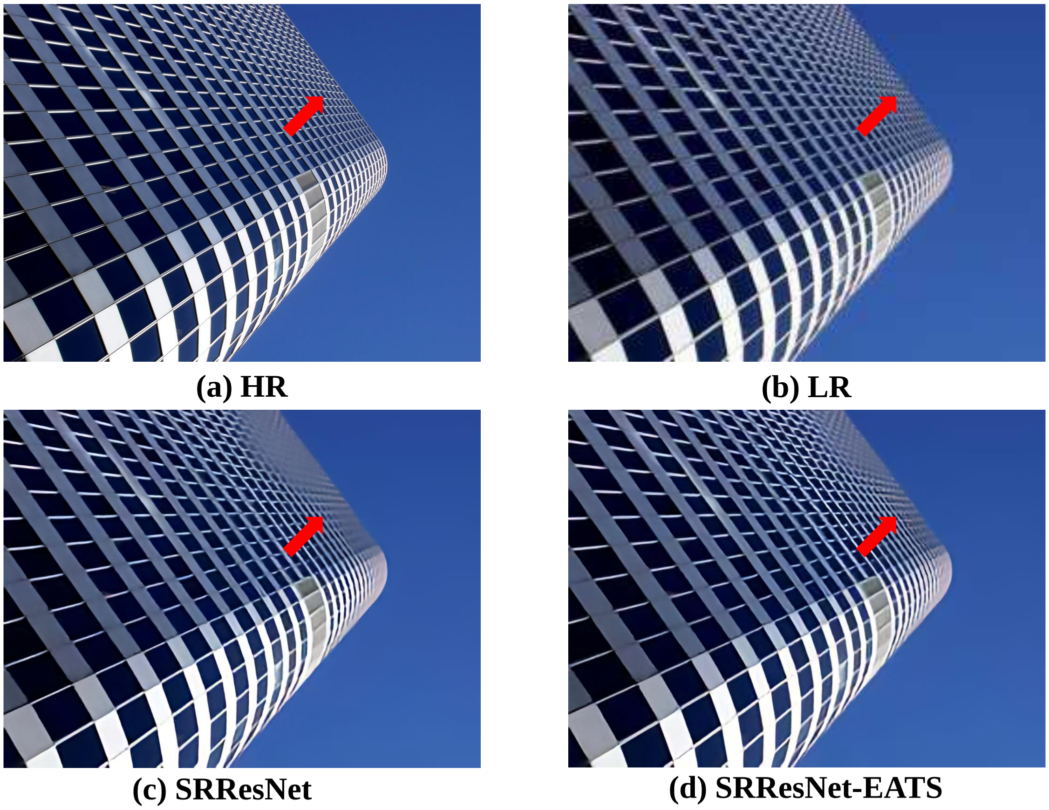

Figure 13: Visual comparison of SRResNet Ledig et al. (2017) on the jpeg-Urban100 Huang et al. (2015).

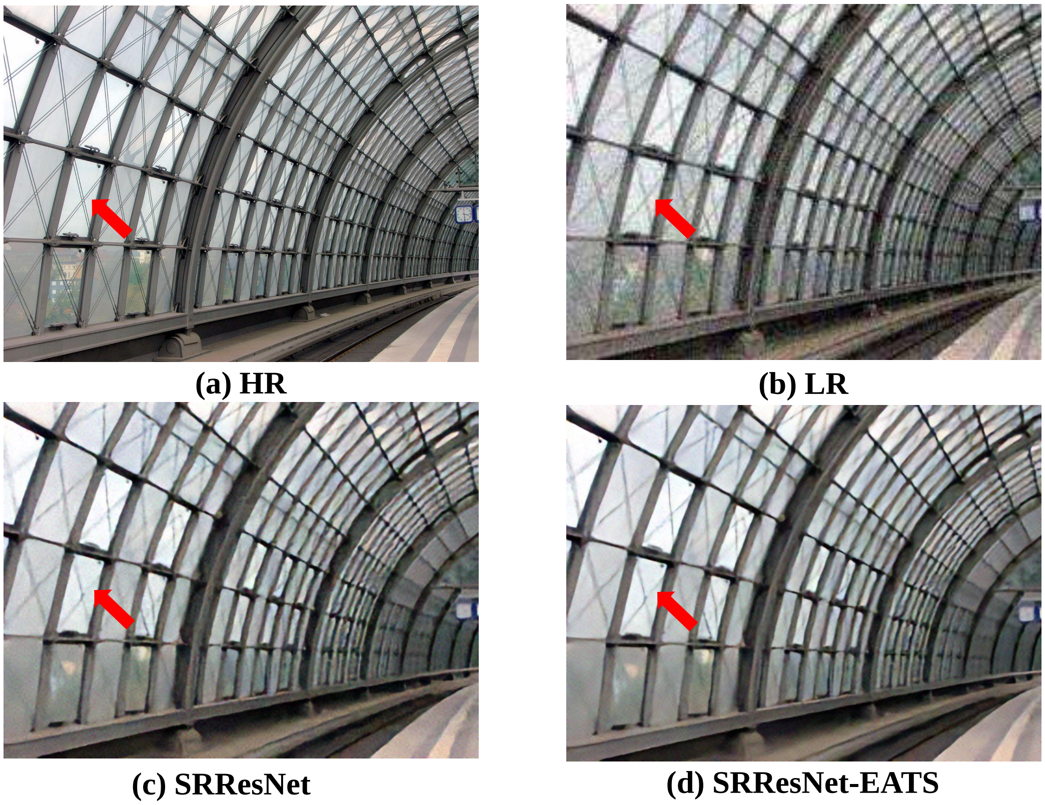

(a) HR

(b) LR

(c) SRResNet

(d) SRResNet-EATS

Figure 14: Visual comparison of SRResNet Ledig et al. (2017) on the blur-noise-Urban100 Huang et al. (2015).

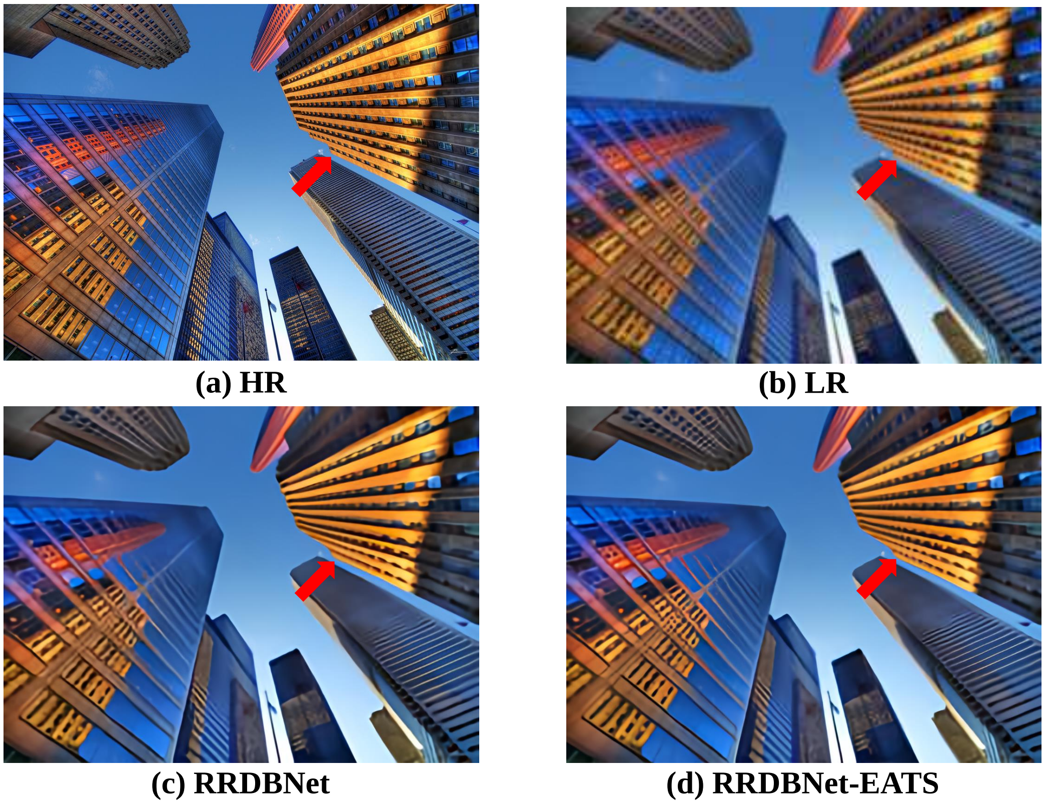

Figure 15: Visual comparison of RRDBNet Zhu et al. (2020) on the blur-jpeg-Urban100 Huang et al. (2015).

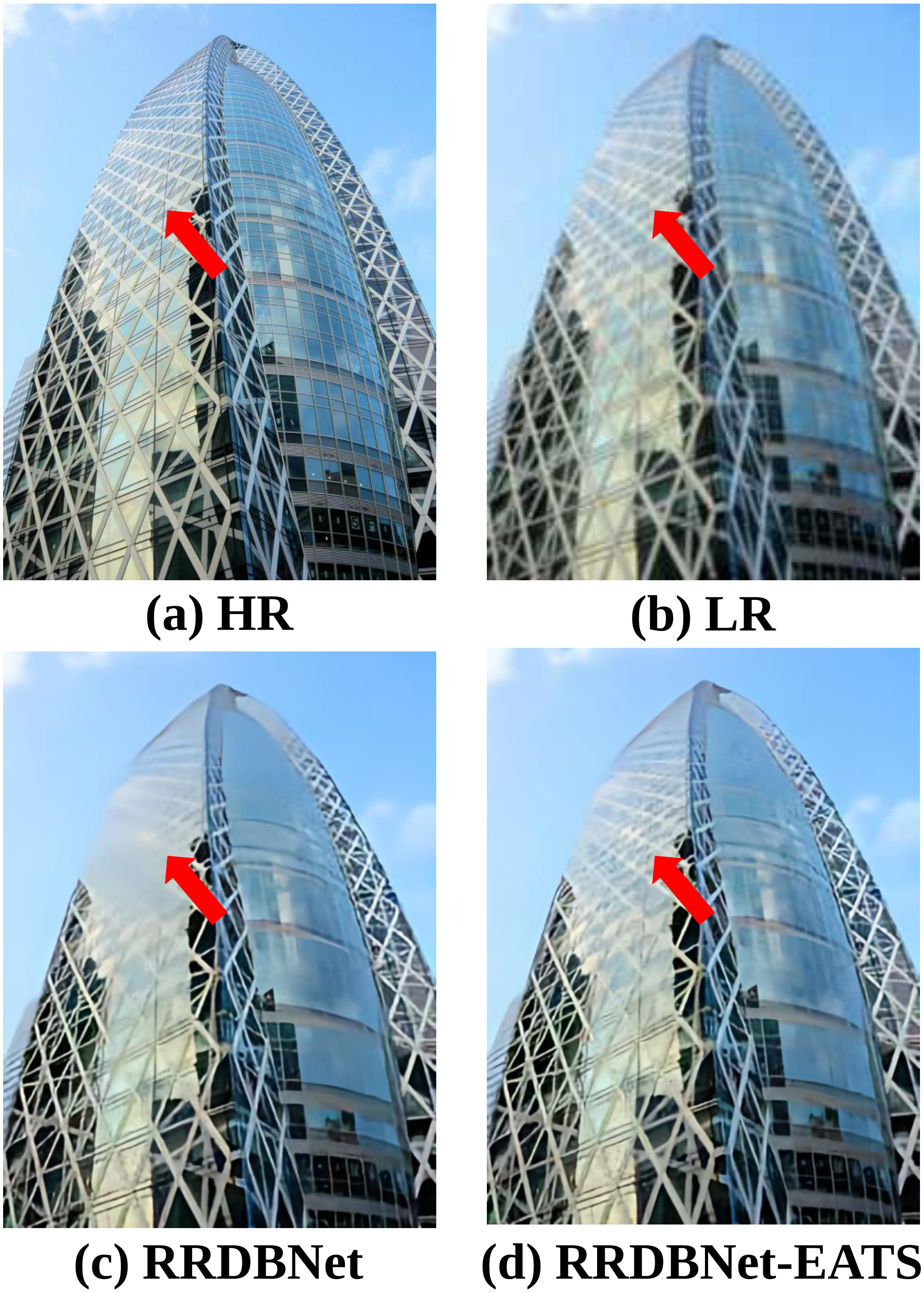

(a) HR

(b) LR

(c) RRDBNet

(d) RRDBNet-EATS

Figure 16: Visual comparison of RRDBNet Zhu et al. (2020) on the noise-jpeg-Urban100 Huang et al. (2015).

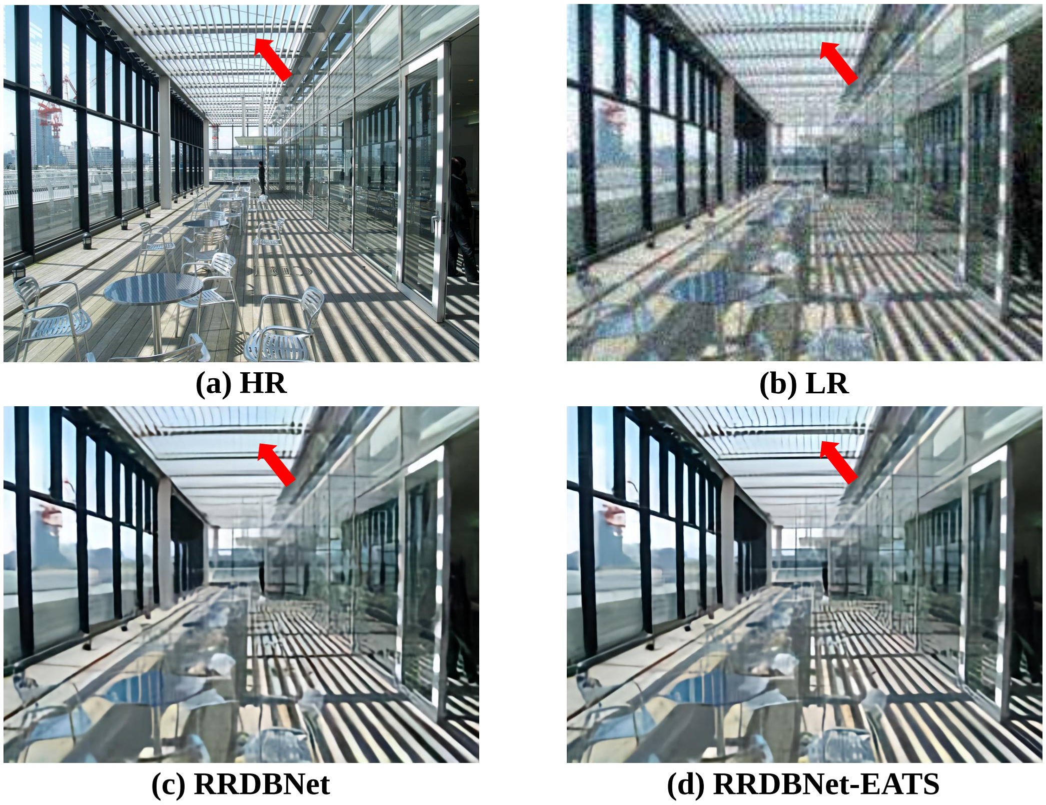

Figure 17: Visual comparison of RRDBNet Zhu et al. (2020) on the blur-noise-jpeg-Urban100 Huang et al. (2015).